Electronic Supplementary Material (ESI) for Dalton Transactions.
This journal is © The Royal Society of Chemistry 2015

Supporting Information for Publication

Chemistry and Structure by Design: Ordered $CuNi(CN)_4$ Sheets with Copper(II) in a Square-Planar Environment

Ann M. Chippindale,*[,a] Simon J. Hibble,*[,b] Edward J. Bilbé,[a] Elena Marelli,[a]

Alex C. Hannon[c] and Mohamed Zbiri

[a] Department of Chemistry, University of Reading, Whiteknights, Reading RG6 6AD, U.K.

[b] Present address: Jesus College, Oxford OX1 3DW, UK

[c] ISIS Facility, Rutherford Appleton Laboratory, Chilton, Didcot OX11 0QX, U.K.

[d] Institut Laue-Langevin, BP 156, F-38042 Grenoble Cedex 9, France

EMAIL ADDRESSES FOR CORRESPONDENCE:

a.m.chippindale@rdg.ac.uk; simon.hibble@rdg.ac.uk

1. Synthesis and Characterisation of Mixed Copper(II)-Nickel(II) Cyanide, $CuNi(CN)_4$

1.1 Synthesis of $CuNi(CN)_4$

Caution! Soluble cyanide compounds can be extremely toxic if inhaled, swallowed or absorbed through the skin. They should be handled with care wearing gloves and safety glasses in a ventilated area, especially when preparing samples of gram quantities needed for neutron diffraction.

$K_2Ni(CN)_4 \cdot nH_2O$ (Aldrich) (5.3020 g, ~0.0220 mol) was dissolved in distilled water (110 ml) and added to an aqueous solution (110 ml) of $CuSO_4 \cdot 5H_2O$ (Aldrich) (5.4899 g, 0.0296 mol) at room temperature. A blue-green gelatinous solid formed immediately. This was stirred for four hours during which time, it turned grey in colour. It was then filtered, repeatedly washed with distilled water and allowed to dry in air. The dry product was in the form of a fine grey powder. The Cu:Ni ratio of 1:1 was confirmed by the total neutron diffraction analysis (Section 2, page S10) and the absence of water by IR and Raman spectroscopy (Section 1.2, page S4) and thermogravimetric analysis (Section 1.4, page S7). Atomic Absorption analysis: Cu:Ni 0.98:1.00. Combustion analysis: Found C: 20.79; N: 23.71; H: < 0.10 % [Calc. for $CuNi(CN)_4$ C: 21.23; N: 24.76; H: 0 Cu: 28.08; Ni 25.93 %]. The powder X-ray diffraction patterns at room temperature and over a range of temperatures are given in Sections 1.3 and 3.2 (pages S6 and S18, respectively).

1.2 IR and Raman Spectra of $CuNi(CN)_4$

Infrared and Raman spectra were measured at room temperature on undiluted powder samples using a Perkin Elmer spectrum 100 FT-IR spectrometer with a Universal Attenuated Total Reflection sampling accessory and a Renishaw InVia Raman microscope (λ_{exc} = 633 nm), respectively (Figures S.1 and S.2).

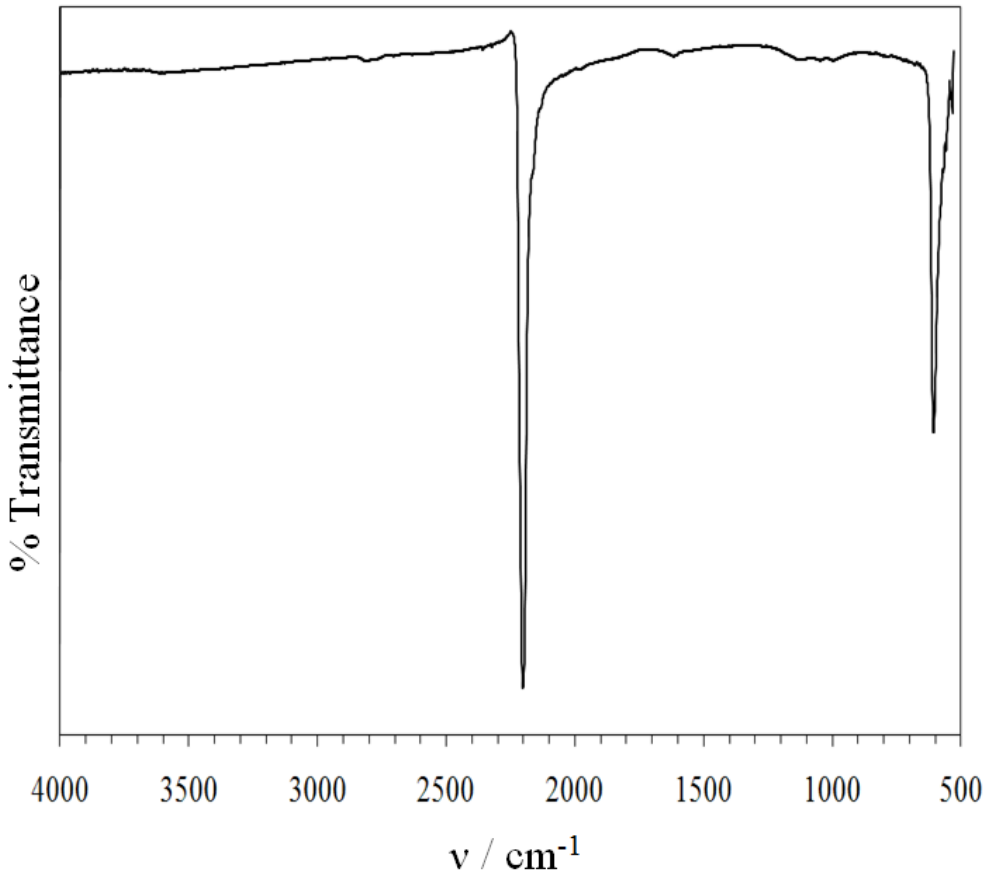

Figure S.1: IR spectrum of grey polycrystalline $CuNi(CN)_4$

(ν(C≡N) 2181(s, broad); ν(Cu–N, Ni–C) 576(w) cm^{-1}).

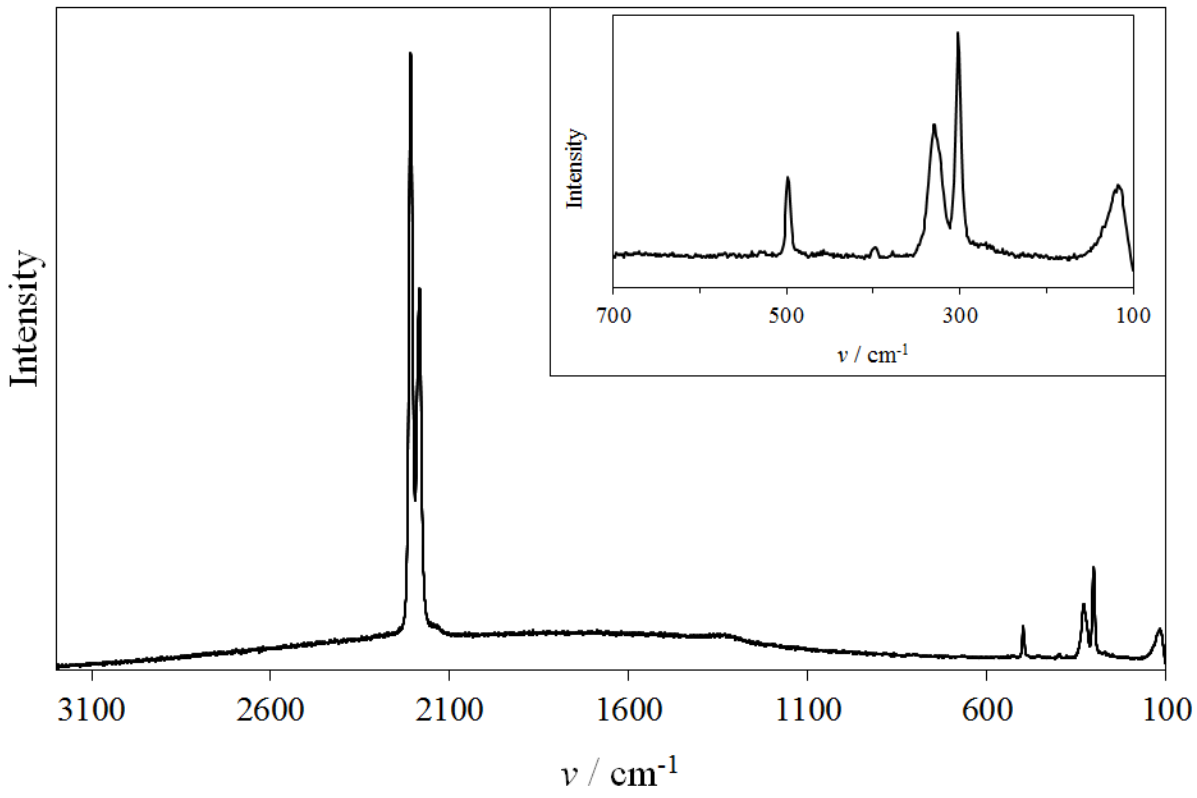

Figure S.2: Raman spectrum of grey polycrystalline $CuNi(CN)_4$

(ν(C≡N) 2209(s), 2184(s); ν(Cu–N, Ni–C) 498 (vw); low frequency bends: 398 (vvw, broad), 329(vw, broad), 301(w), 123(vw, broad) cm^{-1}).

1.3 Room-temperature Powder X-ray Diffraction

Room-temperature powder X-ray diffraction data were measured using a Bruker D8 diffractometer (Cu $K\alpha_1$ radiation, λ = 1.54060 Å) operating in Bragg-Brentano geometry using standard poly(methyl methacrylate) sample holders (Figure S.3).

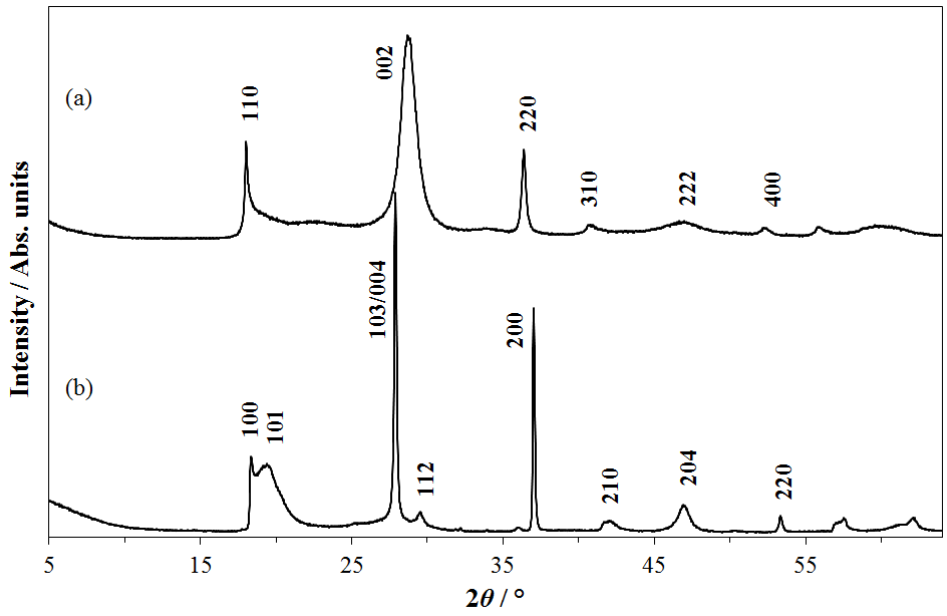

Figure S.3: Powder X-ray diffraction patterns at 295 K of (a) $CuNi(CN)_4$ (a = 6.957(1) and c = 6.180(6) Å) and (b) $Ni(CN)_2$ (a = 4.857 and c = 12.802 Å) (Cu Kα1 radiation, λ = 1.54060 Å)[1].

1.4 Thermal Analysis of $CuNi(CN)_4$

Thermal analyses of $CuNi(CN)_4$, was performed under dry N_2 between 288 and 680 K at a heating rate of 1 K min^{-1} using a TA Q600 STD, simultaneous TGA/DSC instrument (Figure S.4).

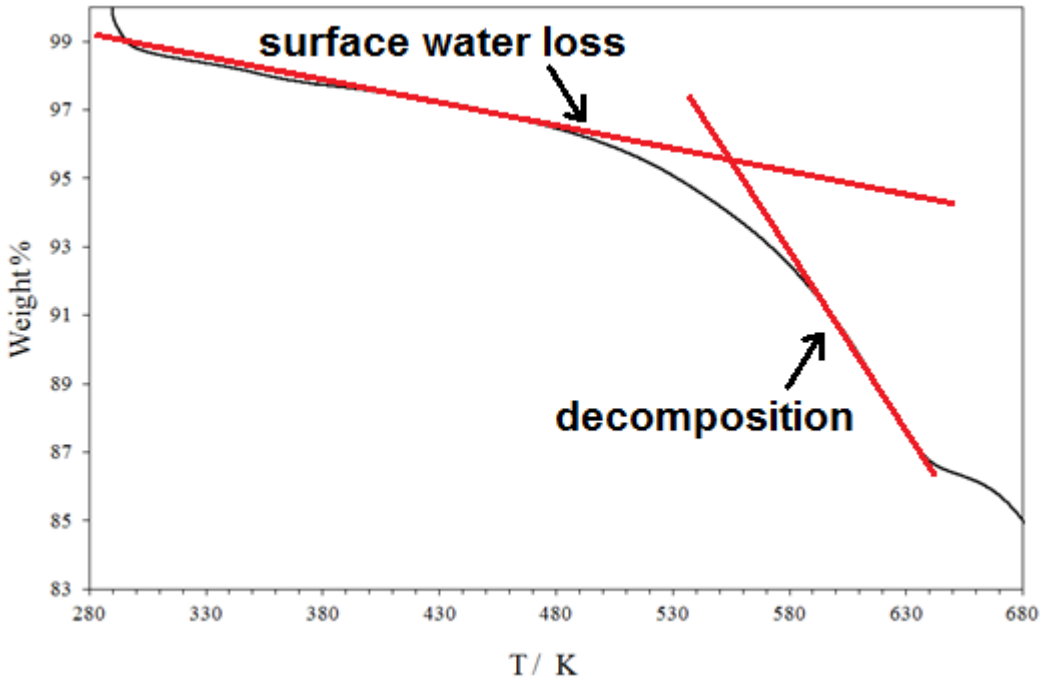

Figure S.4: TGA over the range 288-680 K for $CuNi(CN)_4$. The initial weight loss is due to surface water followed by decomposition from ~565 K.

The IR spectrum of the dark-brown product (Figure S.5), shows peaks at 2200(s) and 2169(s) cm^{-1}, which agree well with the literature values of 2199 and 2170 cm^{-1} for ν(C≡N) for $Ni(CN)_2$[1] and HT–CuCN,[2] respectively. The broad peak at 1350 cm^{-1} is assigned to ν(C=N) of paracyanogen, $(C=N)_n$,[3] the polymeric form of cyanogen, $(CN)_2$, which has been observed previously as a product on heating mercuric cyanides.[4, 5] The formation of paracyanogen also explains the dark colour of the heated product. The powder X-ray diffraction pattern of the final product clearly contains peaks from $Ni(CN)_2$[1] and HT–CuCN[2] (Figure S.6) (N.B. paracyanogen, a disordered polymer, has no observable peaks in the diffraction pattern).

Thus at 635 K under N_2, the overall reaction is: $Cu^{II}Ni(CN)_4 = Ni(CN)_2 + Cu^{I}CN + (CN)_n$

The loss of one cyano group as ½$(CN)_2$ from $CuNi(CN)_4$ has a calculated weight loss = 11.50%.

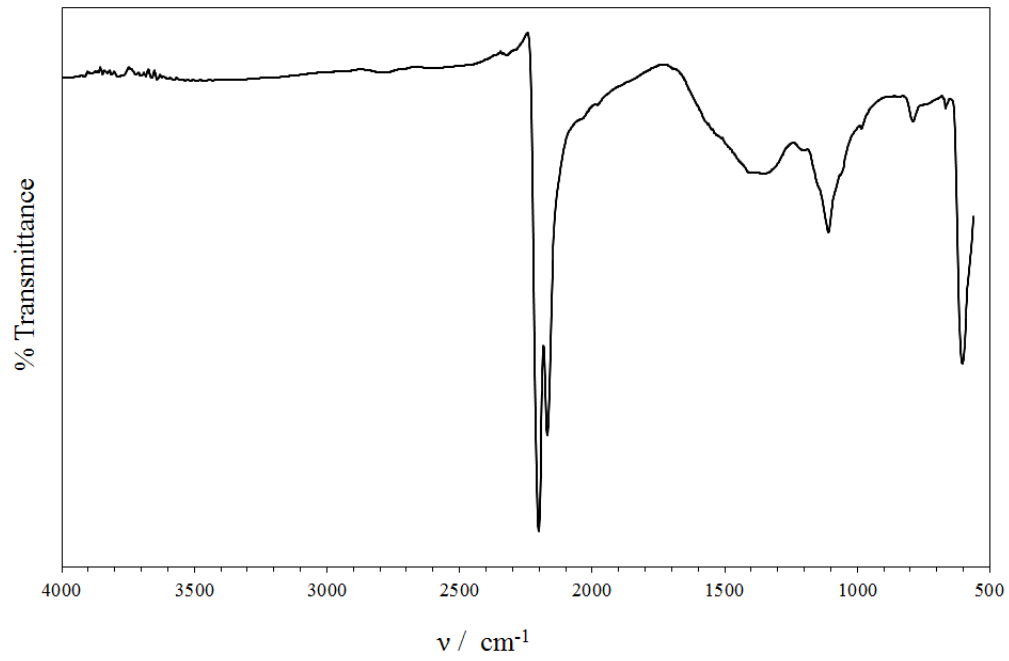

Figure S.5: IR spectrum of the product formed after heating $CuNi(CN)_4$ under N_2 in thermogravimetric balance. The peaks at 2200(s) and 2169(s) cm^{-1}, agree well with the literature values for ν(C≡N) for $Ni(CN)_2$[1] and HT–CuCN.[2]

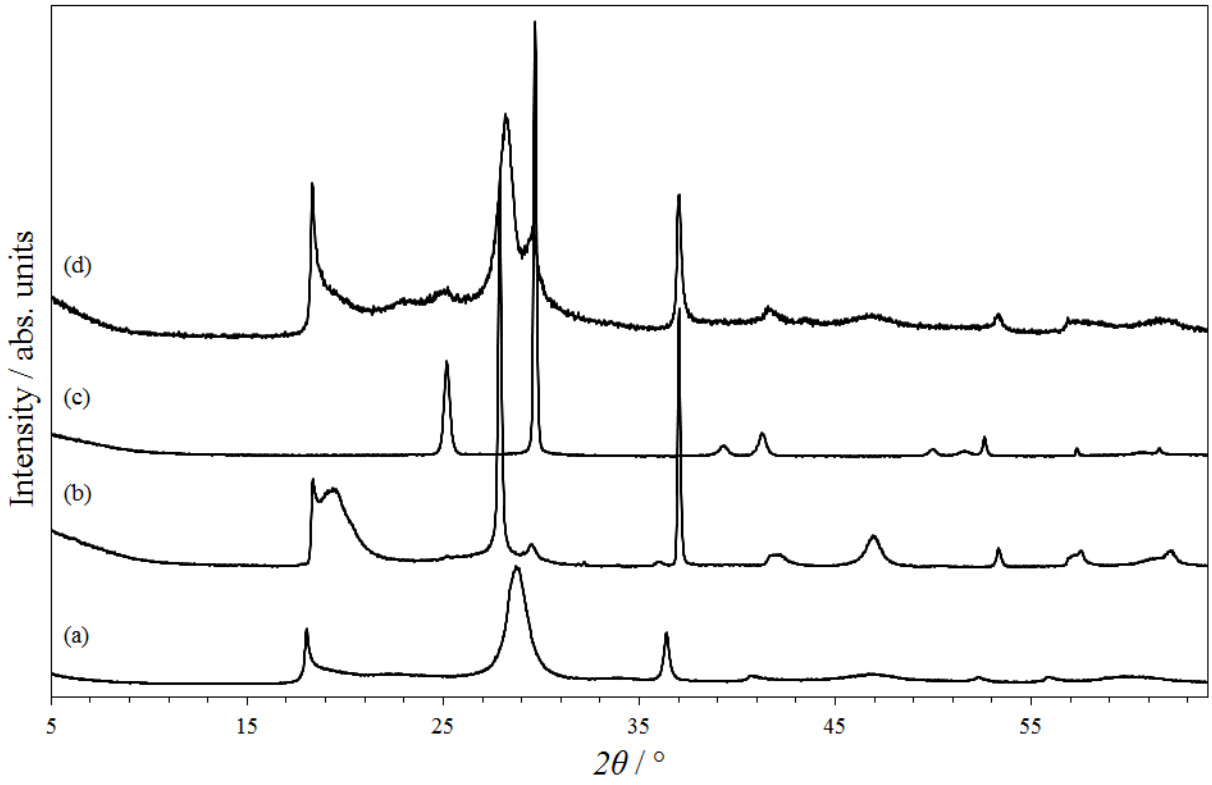

Figure S.6: Powder X-ray diffraction patterns of (a) $CuNi(CN)_4$, (b) $Ni(CN)_2$, (c) HT–CuCN and (d) the product on heating $CuNi(CN)_4$ to 680 K under N_2.

1.5 Magnetic and Diffuse Reflectance Measurements

The magnetic moment of $CuNi(CN)_4$ was measured over the range ($1.83 \leq T$ / K ≤ 350) using a SQUID magnetometer by Dr R. K. Kremer, Max-Planck Institut für Festköperforschung, Stuttgart (Figure S.7).

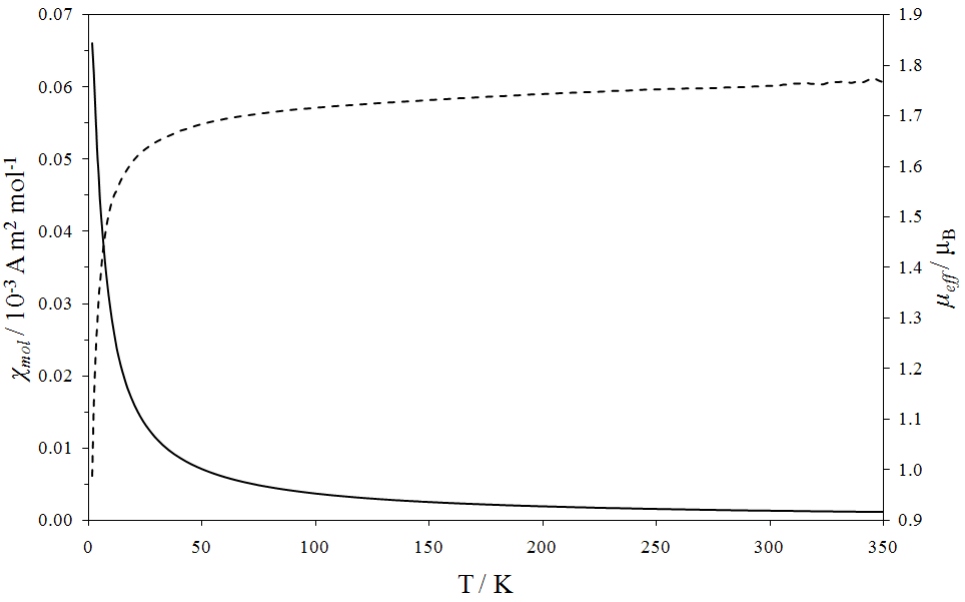

Figure S.7: Molar magnetic susceptibility, χ_{mol} (solid line), and effective magnetic moment, μ_{eff} (dashed line) measured for $CuNi(CN)_4$ over the temperature range 1.83-350 K.

The effective magnetic moment, μ_{eff}, at 295 K is 1.76 μ_B.

Diffuse reflectance spectra were collected for $CuNi(CN)_4$ and $Ni(CN)_2$ over the range 4000 – 49000 cm^{-1} on a Perkin Elmer 900 UV-Vis-NIR spectrometer equipped with a 60 mm diameter integrating sphere (Figure 5). The polycrystalline samples were loaded into a black sample holder with a 1 cm quartz window and the reflectance spectrum measured in the form of the Kubelka-Munk function, $f(R)$.[6]

$$f(R) = \frac{(1-R)^2}{2R} = \frac{k}{s} = \frac{Ac}{s}$$

where R is the reflectance, k the absorption coefficient, s the scattering coefficient, A the absorbance and c the concentration of the absorbing species.

2. Neutron Diffraction and Density Studies of $CuNi(CN)_4$

2.1 Pyknometric Density Measurement

The density of $CuNi(CN)_4$ was measured at room temperature using a Quantachrome Micropycnometer with helium gas as the working fluid. The density obtained was 2.439 g cm^{-3} in excellent agreement with the crystallographic density of 2.440 g cm^{-3} calculated using the unit-cell parameters determined at 295 K (Figure 2) and unit-cell content, Z, equal to 2.

2.2 Neutron Diffraction Studies of $CuNi(CN)_4$

The sample of $CuNi(CN)_4$ (1.7665 g) used in the neutron diffraction experiments was dried at 110 °C under N_2 for 4 hours prior to loading into a 6mm diameter, thin-walled vanadium can under an argon atmosphere.

Time-of-flight total neutron diffraction data were collected on the GEM diffractometer[7,8] at the ISIS facility, Rutherford Appleton Laboratory, Chilton, UK. The vanadium can containing the sample was placed in the instrument sample tank inside a close-circuit refrigerator (CCR). Data were collected at both 15 and 295 K using this experimental setup. The packing densities used in the data correction process were determined from the weight of the samples and can dimensions. Background runs to correct the data were collected on the empty instrument, empty can and on a standard vanadium rod. The data from detector banks 2, 3, 4 and 5 at mean scattering angles 17.3, 34.3, 61.7 and 91.8° were corrected for multiple and backscattering, attenuation and inelasticity and normalized to absolute scattering cross-section units using the program GudrunGUI[9] and the magnetic self scattering derived from the Cu^{2+} (d^9) atoms was subtracted to obtain the final distinct scattering.

The corrected data were merged to yield an interference function, $Qi^N(Q)$, over the Q range 0.7 – 49 $Å^{-1}$ using the suite of programs ATLAS[10] in OpenGenie.[11] The low r region was extrapolated to Q = 0 $Å^{-1}$ using a quadratic function applied to the data between 0.7 and 1 $Å^{-1}$ (Figure S.8).

The interference function was then multiplied by the Lorch modification function[12] before the total correlation function, $T^N(r)_{exp,}$ was obtained *via* Fourier transformation (Figure S.9). Use of the Lorch function eliminates termination ripples in $T^N(r)_{exp}$. The total correlation function, $T^N(r)_{exp}$, obtained in this manner was used in the modelling studies (Section 2.3). N.B. The coherent scattering lengths, $\bar{b}$, for used for Cu, Ni, C and N were 7.718, 10.3, 6.646 and 9.36 fm respectively.[13]

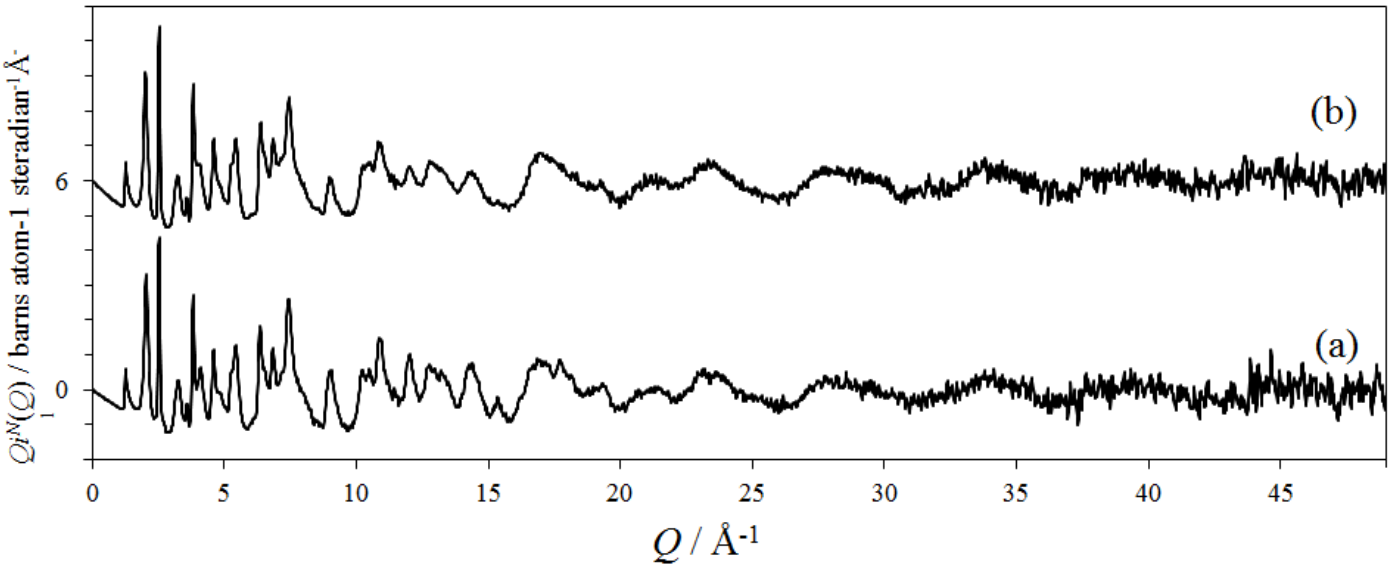

Figure S.8: The interference function, $Qi(Q)$, for $CuNi(CN)_4$ from neutron scattering at (a) 15 K and (b) 295 K (offset for clarity by 6 barns atom^{-1} steradian^{-1}Å^{-1}).

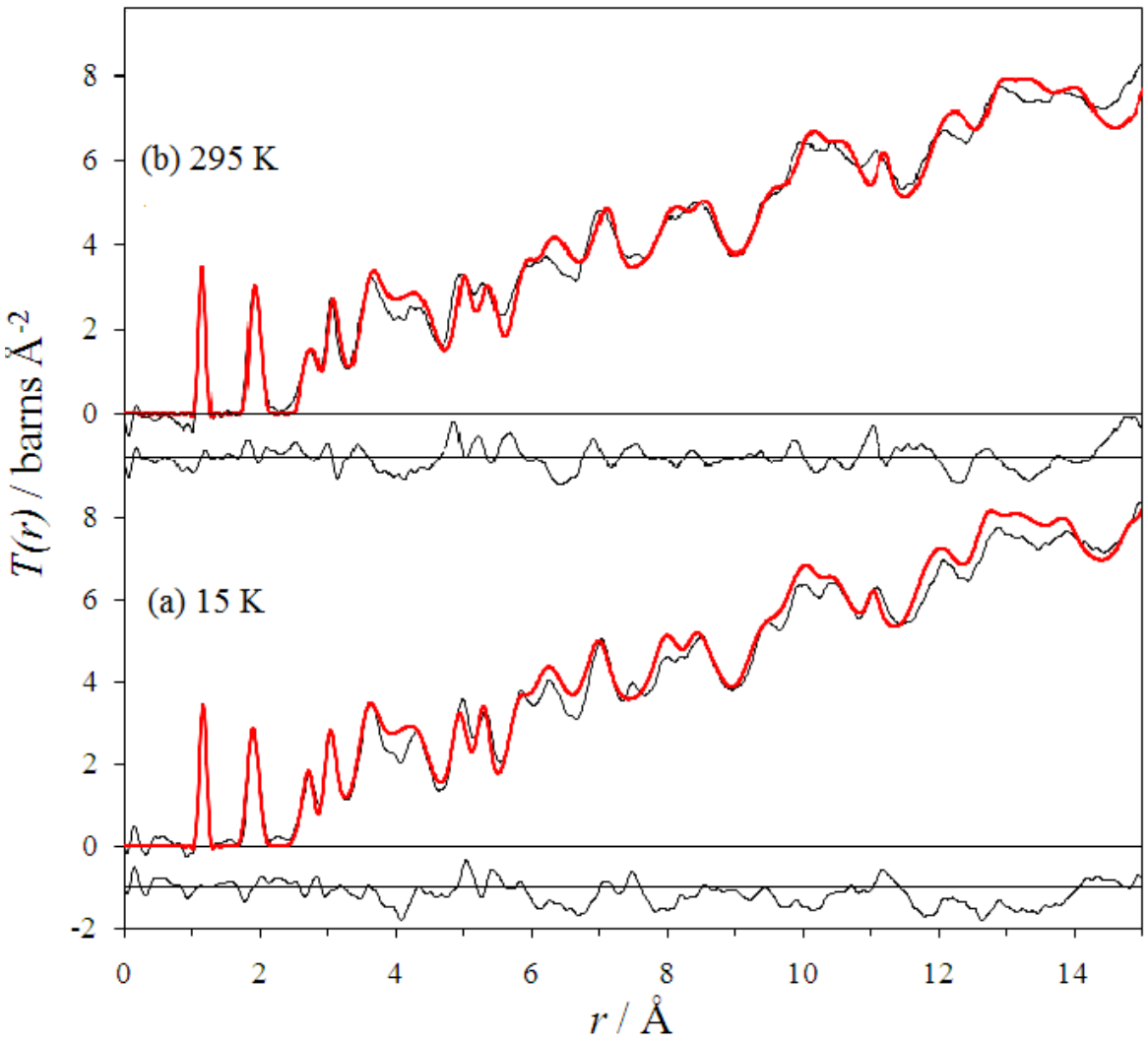

Figure S.9: Total correlation functions, $T^N(r)_{exp,}$ (black line) and $T^N(r)_{mod}$ (red line) for the model in *C mcm*, for $CuNi(CN)_4$ at (a) 15 K and (b) 295 K. The difference function is shown at the bottom of each plot (offset for clarity by 1 barns Å^{-2}).

Figure S.10 shows low-r region of the $T^{N}(r)$ correlation function calculated without using the Lorch function. The advantage of this unmodified transformation is that it is easier to see, particularly in the region $2.5 \leq r$ / Å ≤ 3, that the cyanide linkages must be arranged in the sense Ni–C≡N–Cu in $CuNi(CN)_4$. However, this figure does show large termination ripples that can lead to confusion in identifying peaks. Hence the data shown in Figure S.9 was used for structural modelling.

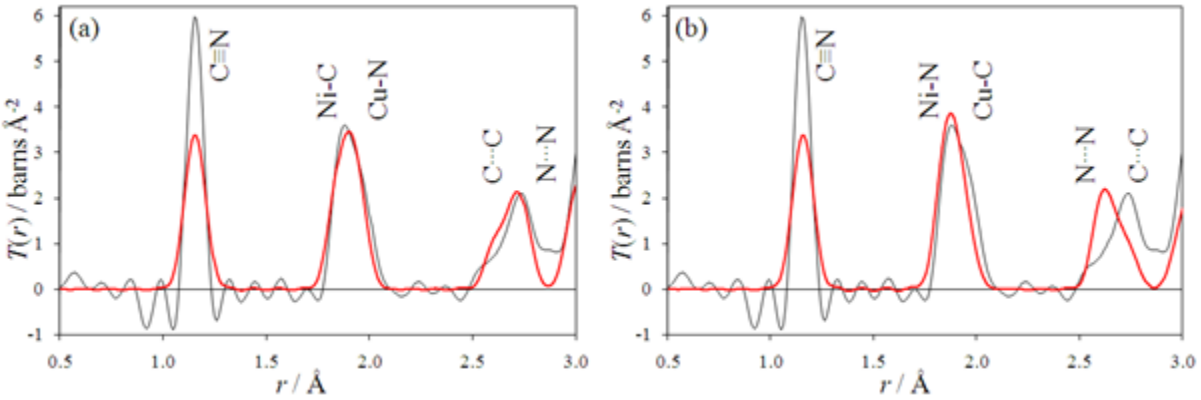

Figure S.10: The low-r region of the $T^{N}(r)$ correlation function of $CuNi(CN)_4$ at 15 K calculated using the step function (thin black line). The $T^{N}(r)_{mod}$ (red line) correlation functions are calculated with a broadening factor of 0.05 Å for every correlation (clearly far from ideal for the C≡N correlation). In (a), the model consists of $Ni(CN)_4$ and $Cu(NC)_4$ units linked through Ni–C≡N–Cu bridges and in (b) $Ni(NC)_4$ and $Cu(CN)_4$ units are linked through Ni–N≡C–Cu bridges. Model (a) gives the best fit, particularly at ($2.5 \leq r$ / Å ≤ 3), supporting the proposal that Ni is bonded to C and Cu to N within the layers of $CuNi(CN)_4$.

Table S.1: Fitted peaks positions, *r*, for $CuNi(CN)_4$ at 15 and 295 K from $T^N(r)_{exp}$ (Figure S.9)

	Atomic pair	*r* / Å	
		15 K	295 K
	C≡N	1.1541(6)	1.1541(6)
	Ni–C	1.857(1)	1.859(2)
	Cu–N	1.943(2)	1.947(2)
*a**/ Å[i]		7.006(2)	7.015(3)
a / Å[ii]			6.957(1)

[i] Values calculated as $a^* = \sqrt{2}\,(d_{Cu–N} + d_{C\equiv N} + d_{Ni–C})$ using the sheet model shown in Figure 1

[ii] Value from PXRD pattern at 295 K (Figure 2)

2.3 Modelling $T^N(r)_{exp}$

Using the Cu–N, Ni–C and C≡N distances determined from $T^N(r)_{exp}$ (Table S.1), it is possible to calculate the length of the side of the square structural repeat unit for one layer of $CuNi(CN)_4$, as shown in Figure 1. At 295 K, this length, *a**, is slightly longer than the value, *a*, obtained from powder X-ray diffraction. This discrepancy arises because in calculating *a**, no account is taken of the lateral thermal displacements of the atoms (see ref [14] for further discussion and justification of the use of *a** for modelling of $T^N(r)$ data).

In order to produce a three-dimensional model of the structure of $CuNi(CN)_4$ incorporating the stacking of the layers, it is necessary to chose a larger structural repeat unit within the layer *i.e.*$\sqrt{2} \times a^*$. In this way, a structural model can be constructed in space group *Cmcm* which fits both the short- and medium-range order as indicated by the good fit to $T^N(r)_{exp}$ (Figure S.9). It should be noted that although the space group is

orthorhombic, we use a tetragonal metric. Overall stacking disorder will lead to pseudotetragonal symmetry, even though this is untrue on a local scale.

Table S.2: Fractional atomic coordinates for $CuNi(CN)_4$ at 15 K used to construct the $T^N(r)_{mod}$ in *Cmcm* with $a = b =$ 9.9082 and $c = 6.100$ Å. N.B. all sites are fully occupied

Atom	Site	*x*	*y*	*z*
Ni	4*c*	0	0.6250	1/4
Cu	4*c*	0	0.1250	1/4
C(1)	4*c*	0	0.8124	1/4
N(1)	4*c*	0	0.9289	1/4
C(2)	4*c*	0	0.4376	1/4
N(2)	4*c*	0	0.3211	1/4
C(3)	8*g*	0.1874	0.6250	1/4
N(3)	8*g*	0.1961	0.1250	1/4

R-factor[15], $R_{T(r)} = 6.92$ % ($0 < r \leq 15$) and 6.45 % ($5 \leq r \leq 15$)

where $R_{T(r)} = \left(\sum_i \left(T^N(r_i)_{exp} - T^N(r_i)_{model} \right)^2 \Big/ \sum_i \left(T^N(r_i)_{exp} \right)^2 \right)^{½}$

Table S.3: Root-mean-square, $\langle u^2 \rangle^{1/2}$, values (Å) used to broaden the individual partial correlation functions to calculate the $T^{N}(r)_{mod}$ for $CuNi(CN)_4$ at 15 K.

Atom pairs	Intra-layer correlations		
Ni•••Ni Cu•••Cu	$r \leq 15.0$ Å $\langle u^2 \rangle^{\frac{1}{2}} = 0.1$		
Cu•••Ni	$r \leq 15.0$ Å $\langle u^2 \rangle^{\frac{1}{2}} = 0.07$		
Ni–C Cu–N	$r \leq 3.0$ Å $\langle u^2 \rangle^{\frac{1}{2}} = 0.058$	$3.0 < r \leq 5.0$ Å $\langle u^2 \rangle^{\frac{1}{2}} = 0.08$	$5.0 < r \leq 15.0$ Å $\langle u^2 \rangle^{\frac{1}{2}} = 0.12$
Ni•••N Cu•••C	$r \leq 4.0$ Å $\langle u^2 \rangle^{\frac{1}{2}} = 0.058$	$4.0 < r \leq 6.0$ Å $\langle u^2 \rangle^{\frac{1}{2}} = 0.08$	$6.0 < r \leq 15.0$ Å $\langle u^2 \rangle^{\frac{1}{2}} = 0.18$
C≡N	$r \leq 3.0$ Å $\langle u^2 \rangle^{\frac{1}{2}} = 0.027$	$3.0 < r \leq 6.0$ Å $\langle u^2 \rangle^{\frac{1}{2}} = 0.12$	$6.0 < r \leq 15.0$ Å $\langle u^2 \rangle^{\frac{1}{2}} = 0.18$
C•••C	$r \leq 3.0$ Å $\langle u^2 \rangle^{\frac{1}{2}} = 0.078$	$3.0 < r \leq 15.0$ Å $\langle u^2 \rangle^{\frac{1}{2}} = 0.18$	
N•••N	$r \leq 3.0$ Å $\langle u^2 \rangle^{\frac{1}{2}} = 0.063$	$3.0 < r \leq 15.0$ Å $\langle u^2 \rangle^{\frac{1}{2}} = 0.18$	

Table S.3 (continued)

Atom pairs	Inter-layer correlations		
Ni•••Ni Cu•••Cu Ni•••Cu	$r \leq 7.0$ Å $\langle u^2 \rangle^{\frac{1}{2}} = 0.25$	$7.0 < r \leq 15.0$ Å $\langle u^2 \rangle^{\frac{1}{2}} = 0.3$	
Cu•••N Ni•••C Cu•••C Ni•••N	$r \leq 4.0$ Å $\langle u^2 \rangle^{\frac{1}{2}} = 0.18$	$4.0 < r \leq 7.0$ Å $\langle u^2 \rangle^{\frac{1}{2}} = 0.25$	$7.0 < r \leq 15.0$ Å $\langle u^2 \rangle^{\frac{1}{2}} = 0.35$
N•••C N•••N C•••C	$r \leq 5.5$ Å $\langle u^2 \rangle^{\frac{1}{2}} = 0.2$	$5.5 < r \leq 9.0$ Å $\langle u^2 \rangle^{\frac{1}{2}} = 0.22$	$9.0 < r \leq 15.0$ Å $\langle u^2 \rangle^{\frac{1}{2}} = 0.4$

3. Negative Thermal Expansion Studies of $CuNi(CN)_4$

3.1 Variable-temperature Powder Neutron Diffraction Studies

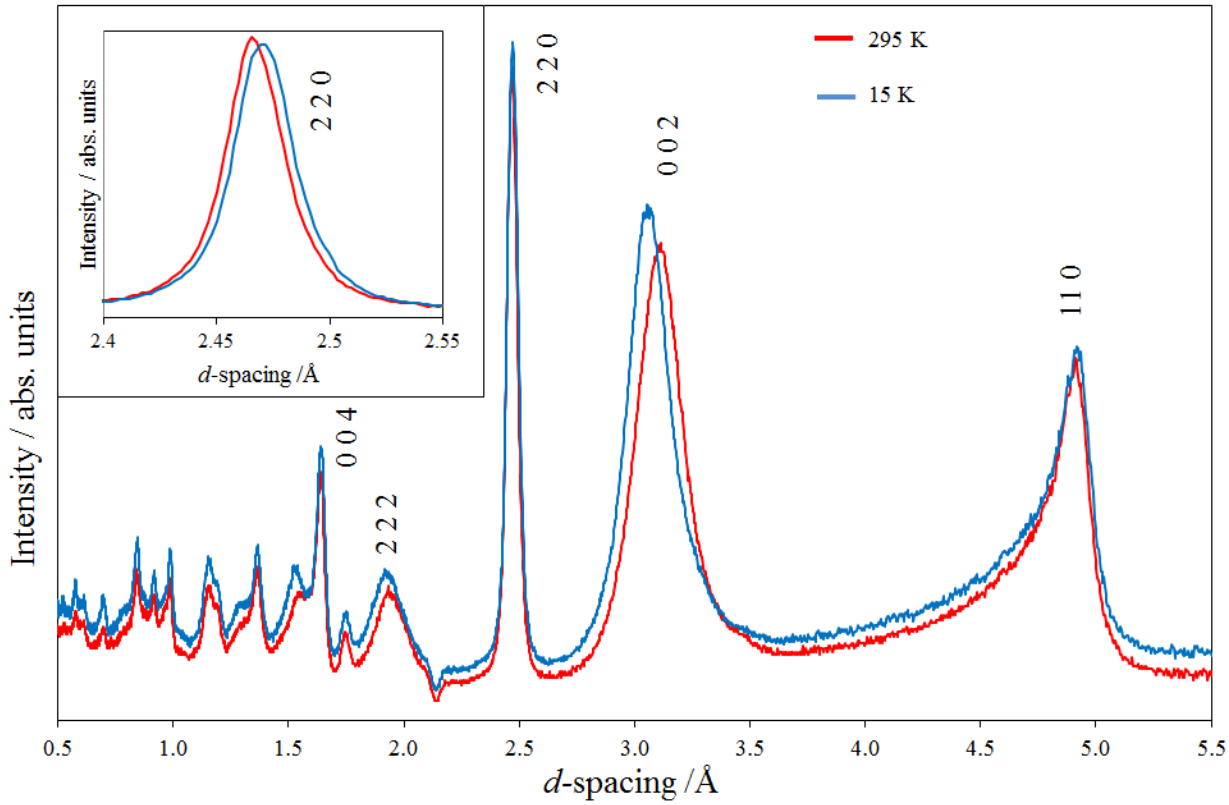

Figure S.11: Powder neutron diffraction pattern of $CuNi(CN)_4$ at 15 K (blue) and 295 K (red) showing the positive thermal expansion along the *c* direction (peak at ~3 Å) and the negative thermal expansion in the *ab* plane (peak at ~4.75 Å) (see inset).

3.2 Variable-temperature Powder X-ray Diffraction Studies

In situ variable-temperature X-ray studies, to investigate the thermal expansion behavior of $CuNi(CN)_4$, were performed using an Anton Parr TTK 450 sample chamber operating under vacuum over the temperature range 93-603 K attached to a Bruker D8 diffractometer (Cu $K\alpha_1$ radiation, λ = 1.54060 Å) (See Figure 6 and Table S.4). $CuNi(CN)_4$ is stable up to 543 K (Figures S.12 and S.13) consistent with the TGA results (Section S.4)

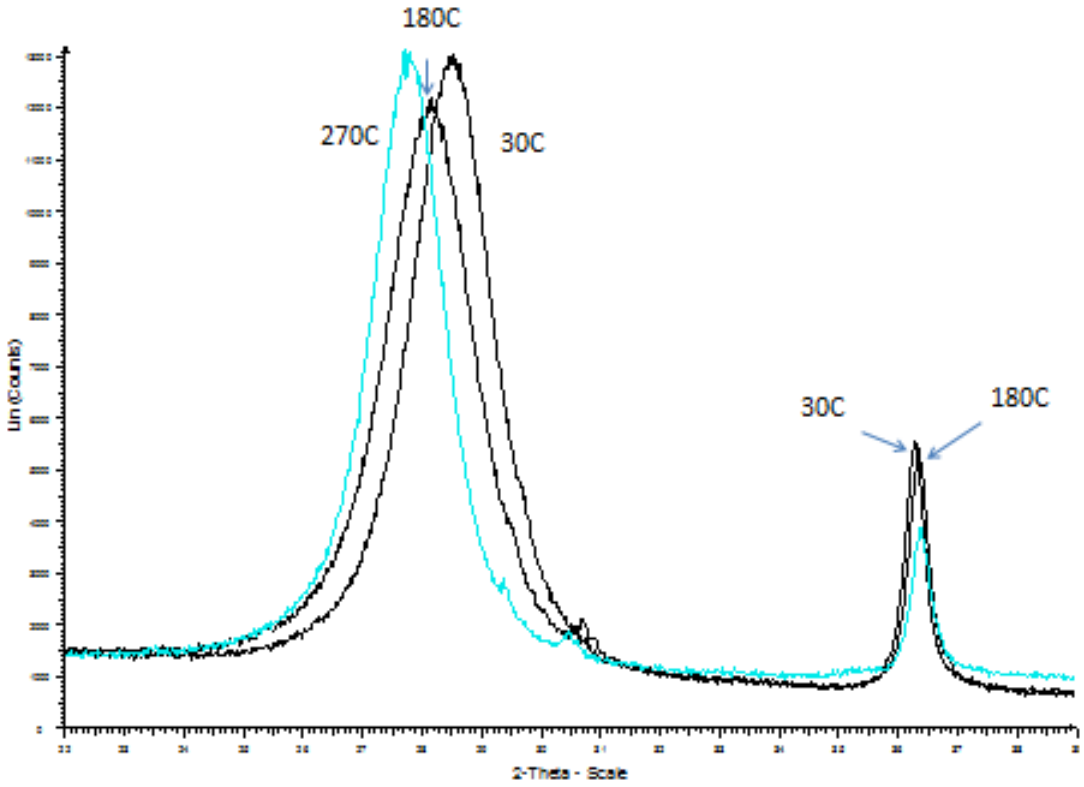

Figure S.12: Powder X-ray diffraction patterns of $CuNi(CN)_4$ at 30, 180 and 270 °C (303, 453 and 543 K) showing the positive thermal expansion along the *c* direction ((002) peak at 2θ ~28 °) and the negative thermal expansion in the *ab* plane ((220) peak at ~2θ ~36.5 °)

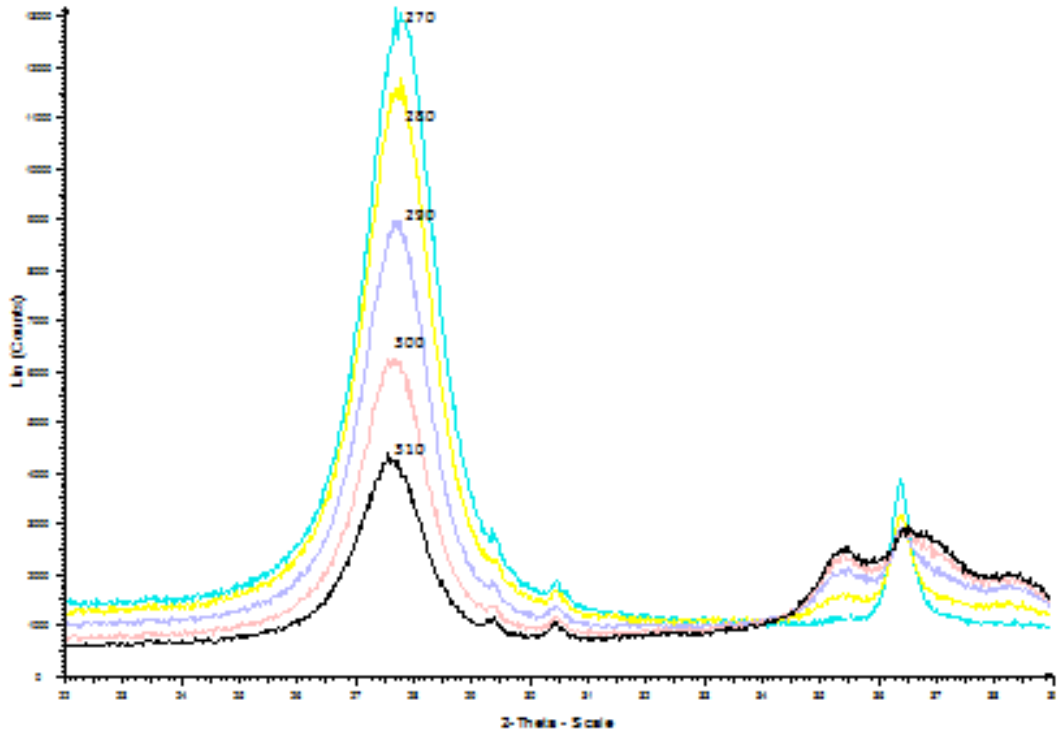

Figure S.13: X-ray diffraction patterns of $CuNi(CN)_4$ over the temperature range 270-310 °C (543-583 K) showing decomposition of the sample.

Table S.4: Linear thermal expansion coefficients for lattice parameters *a* and *c* and unit-cell volume, *V*, for $Ni(CN)_2$ and $CuNi(CN)_4$ measured using powder X-ray diffraction.

	α_a / 10^{-6} K^{-1}	α_c / 10^{-6} K^{-1}	α_V / 10^{-6} K^{-1}	T_{range} / K	Ref.
$CuNi(CN)_4$	–9.7 (8)	89 (9)	70(1)	93 – 543	
$Ni(CN)_2$	–6.5 (1)	68.8 (3)	48.5(5)	12 – 295	[1]
graphene layer	–8.0 (7)			200 – 400	[16]

4. Intercalation of 4,4'-bipyridine into $CuNi(CN)_4$

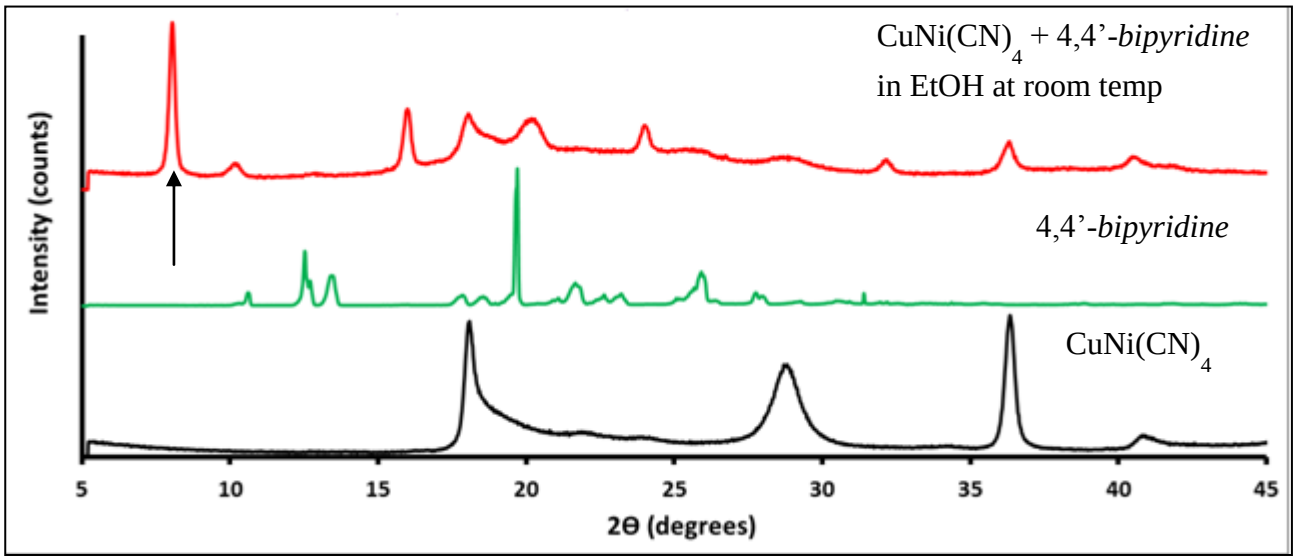

Figure S.14: Powder X-ray diffraction pattern of $CuNi(CN)_4$ after stirring in a solution of 4,4'-bipyridine in ethanol at room temperature for 1 week. Some $CuNi(CN)_4$ still remains in the final product but the appearance of a peak at ~11.3 Å corresponds to an increase in the interlayer separation consistent with intercalation of 4,4'-bipyridine between the $CuNi(CN)_4$ layers.

5. Exploring the Cu(II)-Ni(II)-CN Phase Diagram

5.1 Synthesis of Mixed Copper(II)-Nickel(II) Cyanide Hydrates, $Cu_xNi_{1-x}(CN)_2 \cdot 3H_2O$

Cu(II)-Ni(II) cyanide hydrates, $Cu_xNi_{1-x}(CN)_2 \cdot 3H_2O$ ($0 \leq x \leq 0.25$) were prepared from mixtures of metal chlorides with Cu:Ni ratios of less than 1:3 (Table S.5).

Aqueous solutions of $CuCl_2 \cdot 2H_2O$ and $NiCl_2 \cdot 6H_2O$ were prepared in separate flasks. These were quickly and simultaneously added to an aqueous solution of KCN. In each case, a green gelatinous precipitate immediately formed. The products were stirred for 10 hours, then filtered, washed with distilled water and allowed to dry in air. The resulting fine green powders were characterized using atomic absorption spectroscopy (Table S.5), IR and Raman spectroscopy (Table S.6) and powder XRD (Figure S.15, Table S.7). The powder X-ray diffraction patterns closely resemble that previously measured for $Ni(CN)_2 \cdot 3H_2O$.[17] TGA analysis further confirmed the compositions as $Cu_xNi_{1-x}(CN)_2 \cdot 3H_2O$. Similar reactions using reagents with Cu:Ni ratios between 1:1 and 1:3 produced a mixture of $CuNi(CN)_4$ ($Cu_{0.5}Ni_{0.5}(CN)_2$) and $Cu_{0.25}Ni_{0.75}(CN)_2 \cdot 3H_2O$ ($CuNi_3(CN)_8 \cdot 12H_2O$). The powder XRD pattern of the product of the attempted synthesis of $Cu_{0.375}Ni_{0.625}(CN)_4 \cdot 3H_2O$ clearly shows a mixture of phases (Figure S.16).

Table S.5: Preparation of the mixed Cu(II)-Ni(II) cyanide hydrates, $Cu_xNi_{1-x}(CN)_2 \cdot 3H_2O$

Composition	$CuCl_2 \cdot 2H_2O$	$NiCl_2 \cdot 6H_2O$	KCN	Cu:Ni ratio of reagents	Cu:Ni ratio from AA†
$Cu_{0.05}Ni_{0.95}(CN)_2 \cdot 3H_2O$	0.0343 g (0.20 mmol) in 10 ml H_2O	0.9044 g (3.80 mmol) in 10 ml H_2O	0.5245 g (8.05 mmol) in 10 ml H_2O	0.05	0.05
$Cu_{0.125}Ni_{0.875}(CN)_2 \cdot 3H_2O$	0.0853 g (0.50 mmol) in 15 ml H_2O	0.8312 g (3.50 mmol) in 15 ml H_2O	0.5225 g (8.02 mmol) in 15 ml H_2O	0.14	0.11
$Cu_{0.165}Ni_{0.835}(CN)_2 \cdot 3H_2O$	0.1127 g (0.66 mmol) in 10 ml H_2O	0.7939 g (3.34 mmol) in 10 ml H_2O	0.5220 g (8.02 mmol) in 10 ml H_2O	0.20	0.16
$Cu_{0.25}Ni_{0.75}(CN)_2 \cdot 3H_2O$ ($CuNi_3(CN)_8 \cdot 12H_2O$)	1.1423 g (6.70 mmol) in 75 ml H_2O	4.7800 g (20.1 mmol) in 75 ml H_2O	3.4906 g (53.6 mmol) in 75 ml H_2O	0.33	0.31

† The Cu:Ni ratio in the $Cu_xNi_{1-x}(CN)_2.3H_2O$ phases was verified by atomic absorption spectroscopy. Samples (typically 7-10 mg) were dissolved in 10 ml water containing ~0.02 g of KCN. The solutions were then diluted with distilled water prior to AA analysis using a novAA 350 Analytic Jena spectrometer (with λ = 500 and 341.5 nm for copper and nickel detection, respectively). The estimated standard deviation on the measured values is 2%.

5.2 Infrared and Raman Spectra of $Cu_xNi_{1-x}(CN)_2 \cdot 3H_2O$

Table S.6: IR and Raman spectra of hydrates (frequencies in cm^{-1})

		ν(OH)	ν(C≡N)	δ(HOH)	Low frequency modes
$Cu_{0.05}Ni_{0.95}(CN)_2 \cdot 3H_2O$	IR	3611 (s), 3498 (w), 3257 (w, br)	2165 (vs), 2129 (vw)	1621 (s)	
	R		2185 (vs), 2174 (s)		502 (vw), 448 (vw), 334 (w), 332 (w), 262 (w), 140 (vw)
$Cu_{0.125}Ni_{0.875}(CN)_2 \cdot 3H_2O$	IR	3608 (s), 3495 (w), 3208 (w, br)	2165 (vs), 2125 (vw)	1617 (s)	
	R		2191 (vs), 2178 (s)		502 (vw), 449 (vw), 399 (vw), 332 (w), 266 (w)
$Cu_{0.165}Ni_{0.835}(CN)_2 \cdot 3H_2O$	IR	3611 (s), 3489 (vw), 3257 (w, br)	2165 (vs), 2127 (vw)	1621 (s)	
	R	3623(vvw)	2195 (vs), 2181 (s)		502 (w), 449 (w); 331 (w), 291 (w, sh), 268 (w), 134 (vw)
$Cu_{0.25}Ni_{0.75}(CN)_2 \cdot 3H_2O$ $(CuNi_3(CN)_8 \cdot 12H_2O)$	IR	3612 (w), 3242 (w, v br)	2166 (vs), 2130 (vw)	1616 (s)	
	R		2214 (s), 2194 (vs), 2178(s)		508 (vw), 330 (w, br), 263 (w)
$Ni(CN)_2 \cdot 3H_2O$	IR	3612(s), 3502 (w), 3263 (m, br)	2166(vs), 2125 (vw)	1634(m)	Ref [17]

5.3 Room-temperature Powder X-ray Diffraction Studies of $Cu_xNi_{1-x}(CN)_2 \cdot 3H_2O$

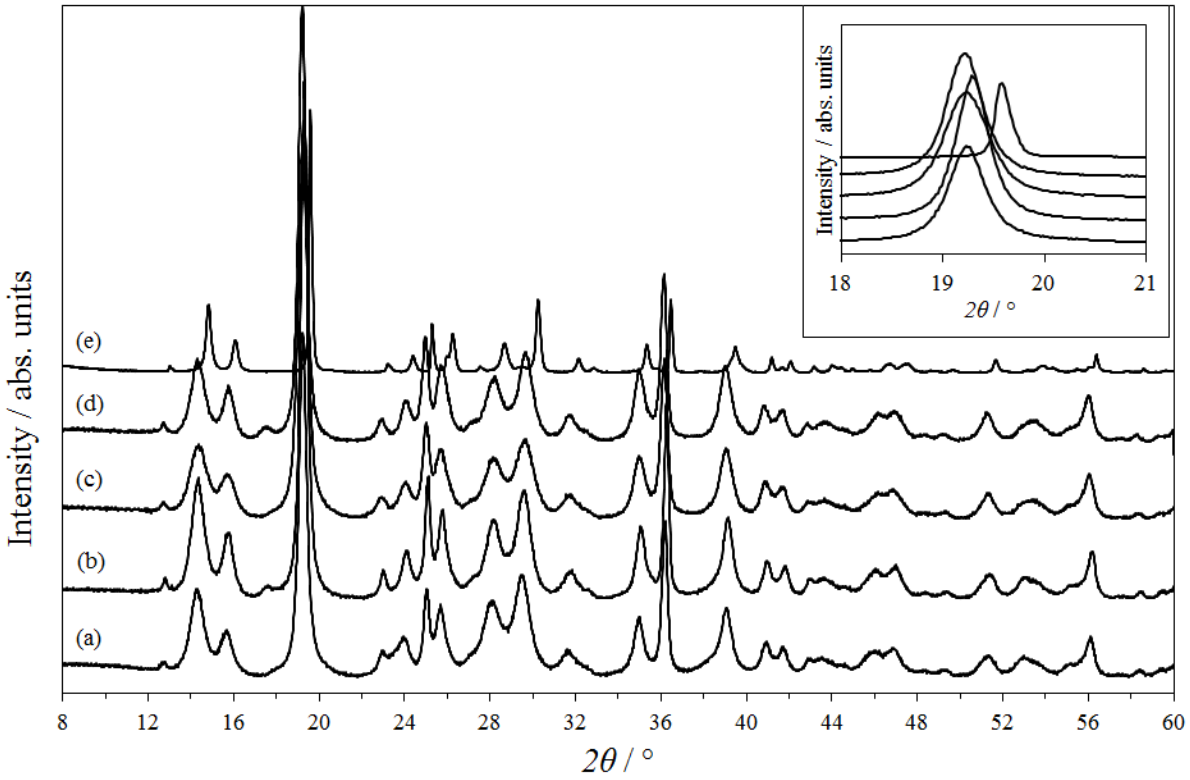

Figure S.15: Powder X-ray diffraction patterns at room temperature of $Cu_xNi_{1-x}(CN)_2 \cdot 3H_2O$: (a) $Cu_{0.25}Ni_{0.75}(CN)_2 \cdot 3H_2O$, (b) $Cu_{0.165}Ni_{0.835}(CN)_2 \cdot 3H_2O$, (c) $Cu_{0.125}Ni_{0.875}(CN)_2 \cdot 3H_2O$ (d) $Cu_{0.05}Ni_{0.95}(CN)_2 \cdot 3H_2O$ and (e) $Ni(CN)_2 \cdot 3H2O$.[17] In the inset, the *2θ* region of 18–21 ° is enlarged for clarity.

Table S.7: Refined lattice parameters for $Cu_xNi_{1-x}(CN)_2.3H_2O$ at room temperature (space group *Pcmn*).

	a /Å	*b* /Å	*c* /Å	*V* /Å^3	Ref.
$Cu_{0.05}Ni_{0.95}(CN)_2 \cdot 3H_2O$	7.0459(9)	13.869(1)	12.366(1)	1208.4(2)	
$Cu_{0.125}Ni_{0.875}(CN)_2 \cdot 3H_2O$	7.051(1)	13.886(1)	12.361(1)	1210.4(8)	
$Cu_{0.165}Ni_{0.835}(CN)_2 \cdot 3H_2O$	7.0754(7)	13.860(2)	12.377(2)	1213.8(2)	
$Cu_{0.25}Ni_{0.75}(CN)_2 \cdot 3H_2O$ ($CuNi_3(CN)_8 \cdot 12H_2O$)	7.074(1)	13.874(2)	12.372(2)	1214.2(3)	
$Ni(CN)_2 \cdot 3H_2O$	7.1261(4)	13.8696(9)	12.2258(7)	1208.4(1)	[17]

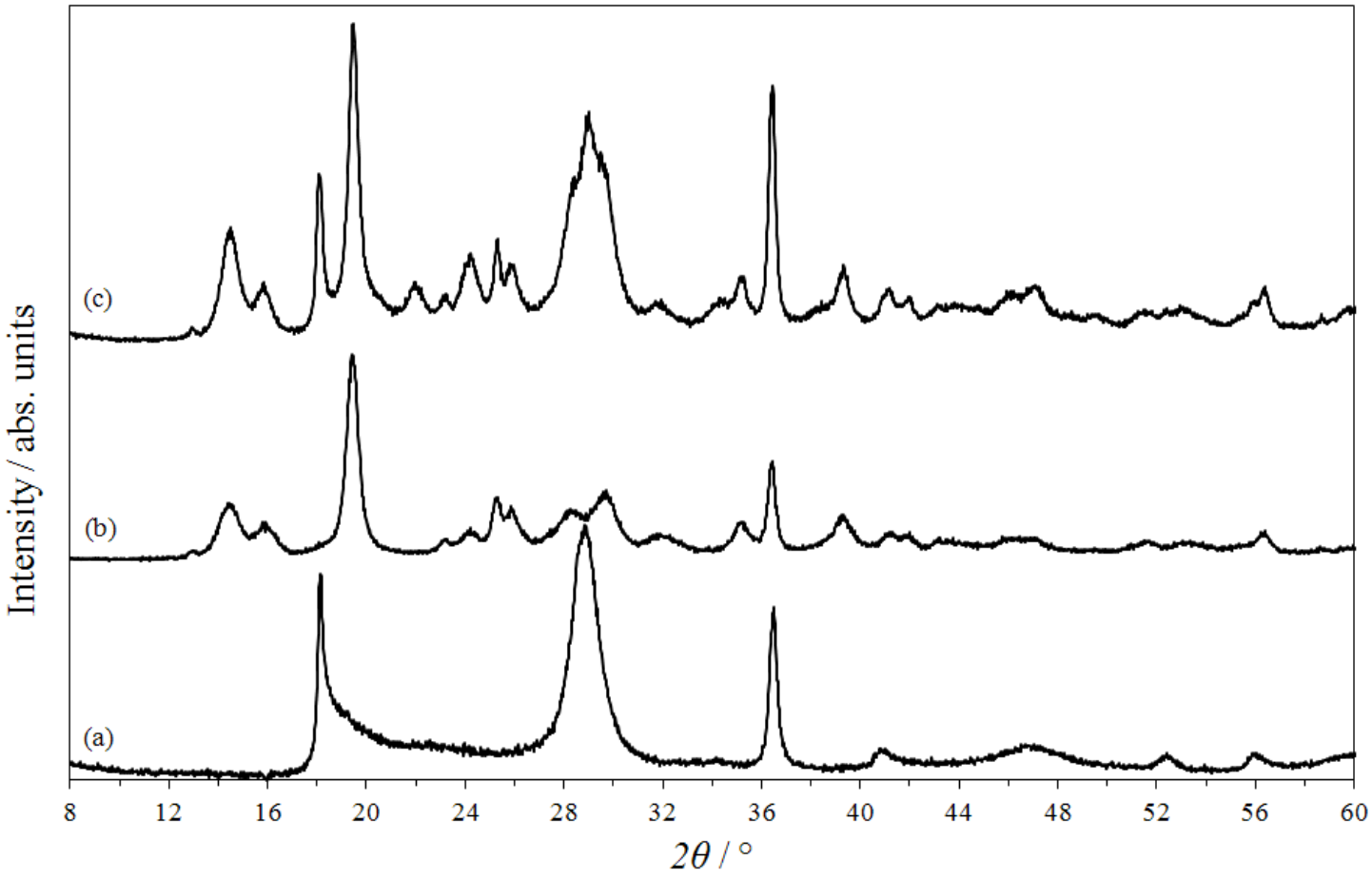

Figure S.16: Powder X-ray diffraction patterns at room temperature of (a) $CuNi(CN)_4$, (b) $Cu_{0.25}Ni_{0.75}(CN)_2 \cdot 3H_2O$ and (c) the product of the reaction of a mixture of $CuCl_2 \cdot 2H_2O$ and $NiCl_2 \cdot 6H_2O$ in KCN with a Cu:Ni ratio of 3:5. Product (c) is clearly a mixture of $CuNi(CN)_4$ and $Cu_{0.25}Ni_{0.75}(CN)_2 \cdot 3H_2O$.

5.4 Preparation and Characterisation of the Dehydrated Phases, $Cu_xNi_{1-x}(CN)_2$ ($0 \leq x \leq 0.25$)

The hydrated phases, $Cu_xNi_{1-x}(CN)_2 \cdot 3H_2O$ ($0 \leq x \leq 0.25$) were dehydrated by heating under vacuum at 400 K for 4 hours. The products were all red/brown in colour and rapidly rehydrated on exposure to moisture. The powder X-ray diffraction patterns were measured *in situ* at 403-413 K, as described in Section 3.2 page S18 (Figure S.17) and closely resemble those of $CuNi(CN)_4$ and $Ni(CN)_2$.

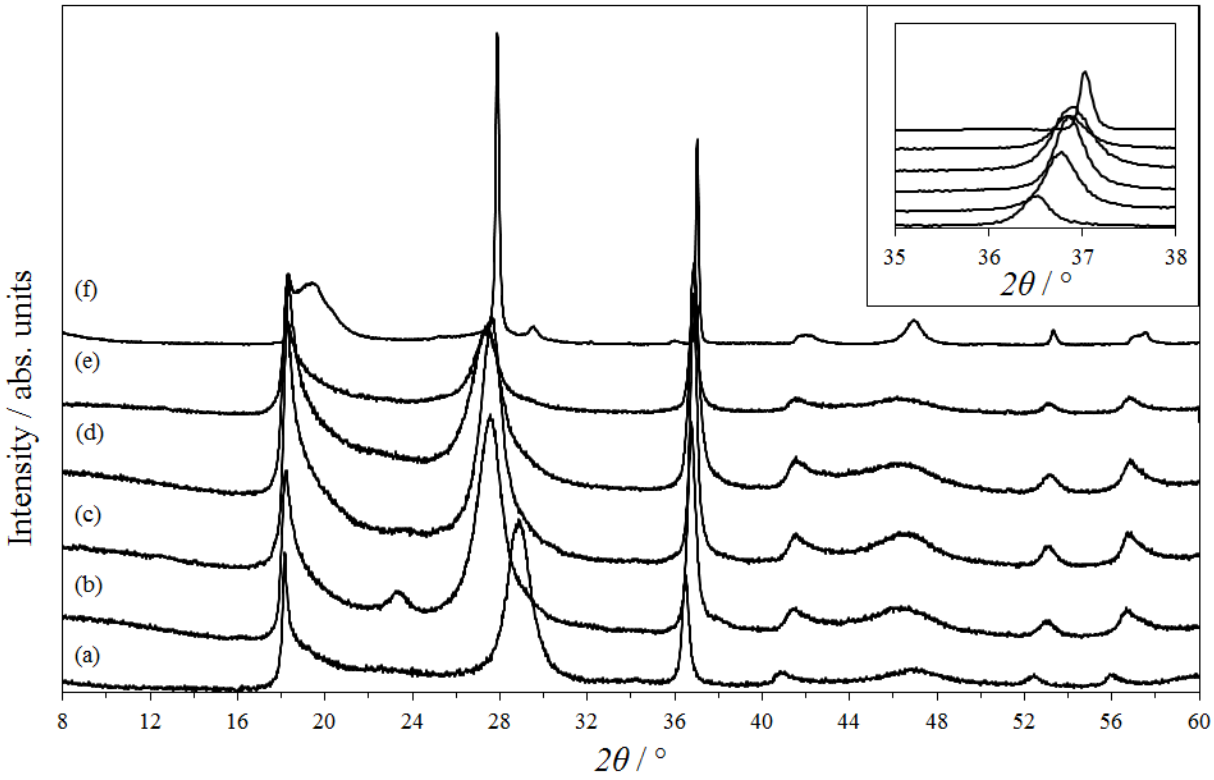

Figure S.17: The room-temperature powder X-ray patterns of (a) $CuNi(CN)_4$, (b) $Cu_{0.25}Ni_{0.75}(CN)_2$, (c) $Cu_{0.165}Ni_{0.835}(CN)_2$, (d) $Cu_{0.125}Ni_{0.875}(CN)_2$, (e) $Cu_{0.05}Ni_{0.95}(CN)_2$ and (f) $Ni(CN)_2$.[1]

5. References

(1) S. J. Hibble, A. M. Chippindale, A. H. Pohl and A. C. Hannon, *Angew. Chem. Int. Ed.*, 2007, **46**, 7116.

(2) S. J. Hibble, S. M. Cheyne, A. C. Hannon and S. G. Eversfield, *Inorg. Chem.*, 2002, **41**, 1042.

(3) F. Cataldo, *Europ. Polym. J.*, 1999, **35**, 571.

(4) G. D. Barrera, J. A. O. Bruno, T. H. K. Barron and N. L. Allan, *J. Phys.: Condens. Matter.*, 2005, **17**, R217.

(5) L. L. Bircumshaw, F. M. Tayler and D. H. Whiffren, *J. Chem. Soc.*, 1954, 931.

(6) P. Kubelka and F. Munk, Z. Tech. Phys., 1931, **12**, 593.

(7) A. C. Hannon in *Encyclopedia of Spectroscopy and Spectrometry* (*eds*. J. Lindon, G. Tranter, J. Holmes) Academic Press: London, 2000; Vol. 2; p 1479.

(8) A. C. Hannon, *Nucl. Instrum. Meth. A*, 2005, **551**, 88.

(9) A. K. Soper, A. C. Hannon, D. T. Bowron, S. E. McLain, *GUDRUN: a program for converting raw diffraction data to differential cross section*, 2006.

(10) A. C. Hannon, W. S. Howells, A. K. Soper, *Inst. Phys. Conf. Ser.*, 1990, **107**, 193.

(11) F. A. Akeroyd, R. L. Ashworth, S. L. Campbell, S. D. Johnston, C. M. Moreton-Smith, R. G. Sergeant, D. S. Silvia, *The ISIS Open Genie user manual*, Vers. 2.0, 1999, RAL-TR-1999-031, Rutherford Appleton Laboratory, Didcot, Chilton, UK

(12) E. Lorch, *J. Phys. C: Solid State Phys.*, 1969, **2**, 229.

(13) V. F. Sears, *Neutron News*, 1992, **3**, 26.

(14) S.J. Hibble, A.M. Chippindale, E. Marelli, S. Kroeker, V.K. Michaelis, B.J. Greer, P.M. Aguiar, E.J. Bilbé, E.R. Barney, and A.C. Hannon, *JACS*, 2013, **135**, 16478.

(15) S. J. Hibble, S. P. Cooper, S. Patat and A. C. Hannon, *Acta Cryst. B*, 1999, **55**, 683.

(16) D. Yoon, Y. W. Son and H. Cheong *Nano Lett.*, 2011, *11*, 3227.

(17) A. H. Pohl, *Solid-state architecture: from simple metal cyanides to open-framework materials*, Ph. D. Thesis, University of Reading, **2008**.